Structural effects on light wave behavior in quasiperiodic regular and decagonal Penrose-tiling dielectric media: A comparative study

Kang Wang*

Laboratoire de Physique des Solides, UMR CNRS/Université Paris-Sud, 91405 Orsay, France
(Received 4 April 2007; published 6 August 2007)

Light wave behaviors in two-dimensional quasiperiodic regular and generalized decagonal Penrose-tiling dielectric media, which display similar long range structure order and different local configurations, are studied comparatively in relation with both global and local orders through the approximant structures. We show that these structures generate analogous photonic band gaps, which are determined by the lattice global average order. Light localization, with frequency levels lying inside the main photonic band gaps, occurs in local regions of high symmetry patterns in the generalized decagonal structure, while it is absent in the regular Penrose tiling. This is analyzed in terms of local symmetry that favors resonances between neighbor scatterers, as well as relations between local and global structure configurations that determine the localized mode frequency levels relative to the photonic band gaps.

I. INTRODUCTION

Quasiperiodic (QP) dielectric media are intensively studied[1–4] both for their potential applications on photonics due to the flatband structures and near-isotropic photonic gaps and their fundamental interest, as these nonperiodic but yet determinist structures provide instructive examples for investigating light wave behaviors in complex dielectric media in relation to structure environments at various scales, especially the effects of global average order and local configurations on photonic gap opening and light localization. Indeed, investigations on photonic states in QP dielectric media have shown that two-dimensional (2D) QP and related dielectric structures can support isotropic band gaps,[1] and that the lowest main photonic band gap is related to the average interplane distance in the dielectric structure.[2] It is also reported that light localization occurs in 2D dielectric QP structure of dodecagonal (12-fold) symmetry inside the photonic band gaps.[3] The same work concluded, however, that the localization phenomenon is absent in 2D QP structures of lower symmetry, namely, the decagonal (tenfold) and octagonal (eightfold) ones, due to long-range correlations. We have shown, in a previous study, that light localization does occur in octagonal QP dielectric structures, but at the band-gap edges, and that the localization mechanism can be attributed to antibonding type local resonances, favored by the high degree of symmetry of the local patterns. Further, dislocalization effect is induced by introduction of disorders through structure randomization. The band structures are, however, not significantly modified.[4]

This raises the general problem of electromagnetic wave behavior in QP dielectric structures, more precisely, the relation between the electromagnetic modes and the QP structures at long- and short-range translational and rotational symmetry orders. A QP structure is generally characterized, at long distance, by quasiperiodic translational order and global average rotational symmetry incompatible with periodicity, and, at local scale, by symmetry centers that display the maximum global rotational symmetry or only the symmetry of a subgroup. For the structures mentioned above, the local-

ization occurs, in the physical space, at local scales on maximum symmetry local centers (respectively 8- and 12-fold rings in the octagonal and dodecagonal structures), indicating local interactions as underlying mechanism. In the frequency spectra, the localized modes have their frequency levels lying inside or at the edge of the photonic band gaps, which in turn depend on the long-range order of the dielectric structure. Indeed, it is proposed that the isotropic photonic band-gap opening is determined by the global translational and rotational orders in octagonal QP structures.[2] Moreover, the relations of the dislocalization effect as well as the band structures to the structure disorders[4] should be considered at both local and global structure scales.

In the present work, we investigate the electromagnetic wave behaviors in relation to both local and global orders in Penrose tiling and related QP structures. Indeed, a comparative study of these different yet intimately related tilings will allow us to understand the structure effects and their consequences on light wave states at different structure scales in QP dielectric media.

II. APPROXIMANT STRUCTURES

Penrose tiling and related structures are probably the best known QP lattices, and the most studied model structures in relation to QP metallic alloys. This family of tilings is interesting for our purpose since it displays various local arrangements with different symmetries under similar long-range global orders. Such structures have been studied as well for various purposes as potential photonic band-gap materials, and most attention are focused on gap properties[5] as well as laser effects[6] and structure-defect related localization.[7] No attention was paid, however, to the structure configuration particularities at global and local scales, and no particular light wave behavior has been reported in relation to different local structure environments.

Indeed, there are many ways to construct Penrose tilings belonging to various local isomorphism classes. We are interested here in two kinds of structures, i.e., the regular Penrose tiling and the generalized decagonal Penrose tiling. Both

these two structures exhibit global average tenfold (C_{10}) symmetry and long-range decagonal bond-orientational symmetry, but with different local configurations. Most notably, the highest local symmetry center in the regular Penrose tiling displays pentagonal (C_5) symmetry, which belongs only to a subgroup of the global average symmetry group, while that in the generalized decagonal Penrose tiling displays C_{10} symmetry, belonging to the maximum global average symmetry group. We will consider the periodic approximant structures of these Penrose tilings, which locally reproduce structure patterns of their parent QP lattices. The latter can, in turn, be successively approached by their approximants of increasing order and size. More importantly, exact solution of Maxwell's equations can be obtained on approximant structures displaying periodic boundary conditions.

Penrose tilings are formed by two kinds of rhombi, both of edge length a, the oblate one with $2\pi/5$ inner angle and the prolate one with $2\pi/10$ inner angle. For simplicity, we will use a direct tiling approach to generate approximant structures. Analogous structures can also be obtained using the cut-and-projection method.[8] Figure 1(a) displays an approximant whose unit cell is in the form of the oblate rhombus. This structure contains 29 nodes per cell, and is characterized by two fundamental lengths $W_{n'}$ and H_n that correspond, respectively, to the width and the height of the cell,

$$W_{n'} = \sqrt{5}a\tau^{n'-2},$$

$$H_n = \sqrt{5}a\tau^{n-1}/\sqrt{1+\tau^2}, \qquad (1)$$

with $n'=4$, $n=5$, and $\tau=(1+\sqrt{5})/2$. It is equivalent to the approximant (4,5) of the regular Penrose tiling in the notation of Ref. 9 and will be referred as such in the following.

Approximants of higher order can be obtained from the (4,5) structure. It is straightforward to construct a higher order approximant structure simply through inflation, by decomposing the rhombus tiles into smaller ones and fitting them together, and introducing periodical tiling mismatches (or "phasons") at the cell boundaries[10] to accommodate the periodicity. Figure 1(b) displays a τ inflated structure (the tiles are decomposed into smaller ones by a factor of τ). The unit cell size corresponds to $(n',n)=(5,6)$ in Eq. (1). This structure will be referred to as the (5,6) approximant of the regular Penrose tiling.

An approximant displaying local tenfold symmetry of the decagonal Penrose tiling can also be obtained from the regular Penrose tiling. To achieve this, we first deflate the (4,5) structure by a factor of $1/\tau^2$ by decomposing the rhombus tiles into larger ones, which are subsequently inflated by a factor of τ^3, so that the final structure is also τ inflated as compared to the (4,5) approximant, but with a different tile rearrangement for the inflation such that the inflated tiling possesses tenfold local environments [Fig. 1(c)]. The obtained structure is locally similar to the τ^3 inflated T_b decagonal tiling obtained through pentagrid method.[11] It has the same size as the (5,6) approximant of the regular Penrose tiling and will be referred to below as the (5,6) approximant of the decagonal Penrose tiling.

(a)

(b)

(c)
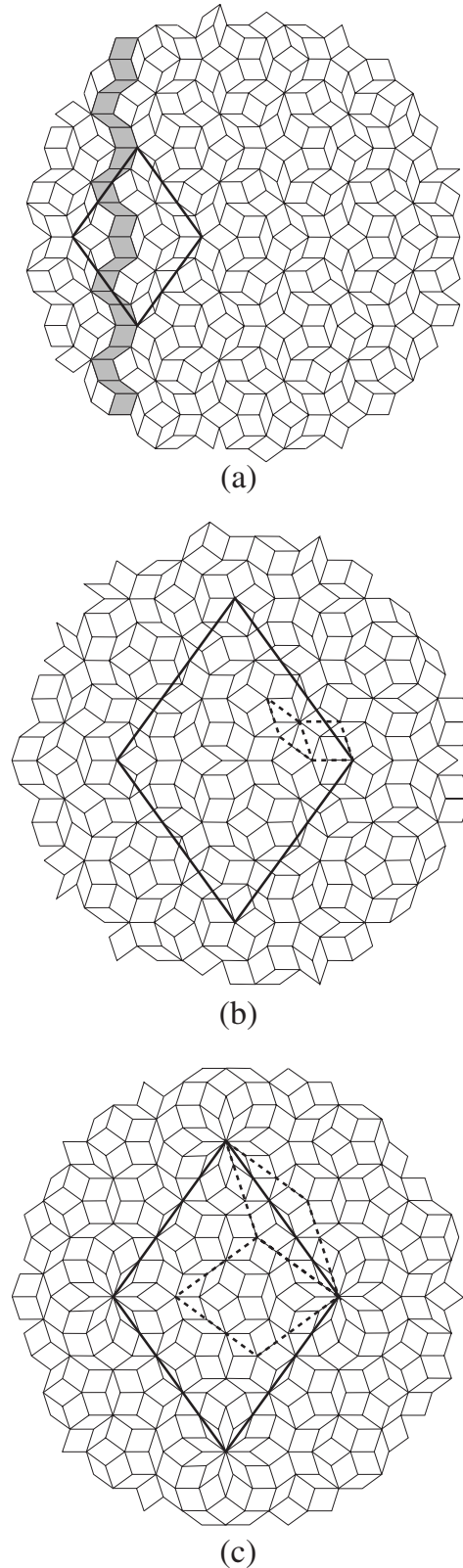
FIG. 1. [(a) and (b)] Two approximants [(4,5) and (5,6)] of the regular Penrose tiling containing, respectively, 29 and 76 nodes. (c) A (5,6) approximant of the decagonal Penrose tiling containing the same number of nodes and the same tiles as (b). The unit cells are indicated by solid lines and the structure-inflation relation by dashed lines. A "ribbon" is shadowed in (a).
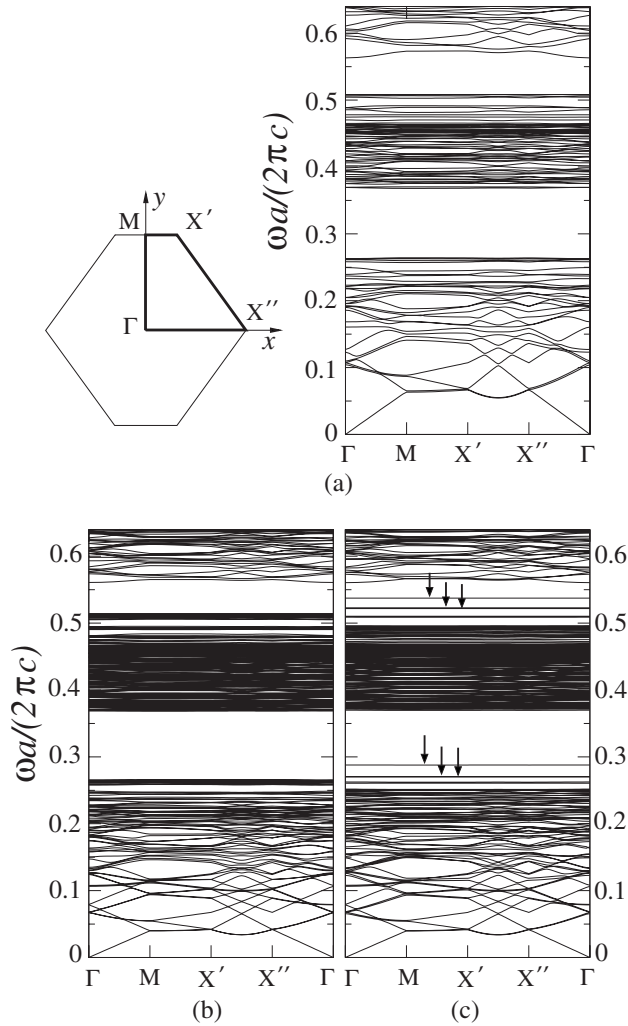
FIG. 2. Band diagrams of [(a) and (b)] the (4,5) and (5,6) approximants of the regular Penrose tiling and (c) the (5,6) approximant of the decagonal Penrose tiling. Arrows in (c) indicate the states inside the two main band gaps; two of them have close frequency levels.

FIG. 3. The Fourier transforms of [(a) and (b)] the (4,5) and (5,6) approximants of the regular Penrose tiling and (c) the (5,6) approximant of the decagonal Penrose tiling. Circles and labels (D1 and D2) indicate the high intensity components responsible for the gap opening.

This simple approach directly yields two (5,6) approximants with unit cells of the same size and containing the same number of lattice nodes (76) as well as the same number of prolate and oblate tiles (29 and 47, respectively). Their structures can be viewed as "isomeric," which are constructed by exactly the same rhombi, but with different local arrangements.

All the three approximant structures display similar global orders, i.e., average pseudo-ten-fold symmetry, decagonal bond-orientational symmetry, as well as similar interline distances (see below). These structures will allow us to investigate the effects of global and local orders on the electromagnetic wave states.

III. LIGHT WAVE BEHAVIORS

The dielectric structures are formed by scatterers that are infinitely high dielectric cylinders of $\epsilon = 13$ and radius $r = 0.24a$. The cylinders are placed perpendicular to the lattice plane at the lattice nodes in an air background, with a corresponding filling rate $f \approx 22\%$ for all the three structures. Maxwell's equations are solved for TM polarization using a plane-wave method. The obtained band diagrams are displayed in Fig. 2. Two main photonic band gaps are obtained for all the three structures. The most notable difference between the regular and decagonal approximants is that, for the decagonal approximant, three modes are shifted into each of the two gaps from the lower frequency ranges as compared to approximants of the regular tiling (this point will be discussed bellow in relation to local structure patterns). As far as the gap characteristics are concerned, all these structures display midgap frequencies of, respectively, about $\bar{\omega}_{gap} \approx 0.32$ and $0.54(\omega a/2\pi c)$ for the two photonic gaps, with comparable gap widths between the structures. Indeed, although the two gaps for the decagonal (5,6) approximant are slightly larger than those for the regular (5,6) approximant, the differences are less than 4%. We note also that the photonic bands outside the gaps have similar structures for the two (5,6) approximants, indicating that light wave propagation in these frequency ranges is not substantially modified by local structure configuration differences.

A. Photonic band gaps

Let us first consider the gap positions in relation to the structure parameters. There are various discussions concerning the gap opening mechanism in Penrose-tiling-related structures.[5] Here, we show that the main photonic gaps can simply be related to the global average order of the dielectric structures through fundamental lattice parameters, though the situation is rather complex due to the tenfold global rotational symmetry of the QP structures that is reduced to a twofold one in passing to approximant structures. The Fourier transforms of these three structures are displayed in Fig. 3. We note that, for all the three approximants, the strong-intensity components are almost identical in positions, their corresponding wave vectors have, therefore, similar magnitudes and directions. Photonic band gaps are determined by strong-intensity Fourier components.[2] Therefore, the fact that the photonic gaps display nearly the same midgap frequencies suggests that it is the strong-intensity Fourier components corresponding to similar wave vectors in the three

TABLE I. The maximum and minimum wave-vector magnitudes for the two pseudodecagonal rings of the Fourier transforms of the (4,5) and (5,6) approximants in Fig. 3, together with the magnitudes of the corresponding wave vectors for the parent QP lattice and those of the two gap wave vectors K_{p_1} and K_{p_2}. All the magnitude values are normalized to $1/a$.

| | Ring vectors | | | | | | |
| | (4,5) | | (5,6) | | | | |
	K_{min}	K_{max}	K_{min}	K_{max}	QP	Gap vectors	
Inner ring	1.205	1.252	1.223	1.241	1.231	K_{p_1}	1.22
Outer ring	1.979	2.008	1.986	1.997	1.992	K_{p_2}	2.05

structures that are responsible for the gap opening.

Indeed, the gap position in a dielectric structure is governed by both dielectric and geometrical parameters. The midgap frequencies ω_{gap} are related to the wave vector K_p on which the gap is opened through the following relations:

$$\omega_{gap}^2 = c^2 k^2/\bar{\epsilon} \tag{2}$$

and

$$k = \frac{1}{2} 2\pi K_p, \tag{3}$$

where $\bar{\epsilon}$ stands for the average dielectric constant.

For the three approximants, the midfrequency of the two main photonic gaps corresponds, respectively, to $K_{p_1} \approx 1.22/a$ and $K_{p_2} \approx 2.05/a$. These values are very close to the average radius of two pseudodecagonal rings defined by two sets of strong-intensity Fourier components [the two component sets for the (4,5) approximant are indicated by circles in Fig. 3(a)]. Indeed, as shown by Table I, where the maximum and minimum values of the wave-vector magnitudes for the two rings are listed for the three approximants, the wave-vector magnitudes of the two pseudodecagonal rings agree well with the two K_p values. This indicates clearly that the gap opening is determined by the Fourier components of the dielectric function corresponding to these wave vectors.

Let us consider two spots, labeled D1 and D2, in each Fourier spectrum in Fig. 3. They are located each on one of the pseudodecagonal rings. Let us refer to the wave vectors on these spots, respectively, as $\mathbf{K}_{D1}^n$ and $\mathbf{K}_{D2}^n$. Their respective magnitudes have the general forms

$$K_{D1}^n = 2F_n/H_n,$$

$$K_{D2}^n = 2F_{n+1}/H_n, \tag{4}$$

with n the approximant order and H_n the unit cell height which is defined in Eq. (1). F_n is the nth order Fibonacci number that can be expressed as

$$F_n = [\tau^n - (-\tau)^{-n}]/\sqrt{5}. \tag{5}$$

We get, for, respectively, the (4,5) and (5,6) approximants, $K_{D1}^5 \approx 1.241/a$, $K_{D2}^5 \approx 1.986/a$ and $K_{D1}^6 \approx 1.227/a$, $K_{D2}^6 \approx 1.994/a$. The wave vectors in an approximant structure are derived from that of the parent QP structure. In the present

case, $\mathbf{K}_{D1}^n$ and $\mathbf{K}_{D2}^n$ are related to two wave vectors, which will be referred to as $\mathbf{K}_{D1}$ and $\mathbf{K}_{D2}$, of the regular and the decagonal QP lattices that have almost identical Fourier transforms. As a matter of fact, $\mathbf{K}_{D1}$ and $\mathbf{K}_{D2}$ are parallel to $\mathbf{K}_{D1}^n$ and $\mathbf{K}_{D2}^n$, and belong each to a set of ten wave vectors ($\mathbf{K}_{\{0,1,1,\bar{1},\bar{1}\}}$ and $\mathbf{K}_{\{0,2,1,\bar{1},\bar{2}\}}$, respectively, in a five-dimensional notation) that point to the vertices of a perfect decagon. Their respective magnitudes are

$$K_{D1} = 2\tau^2/a\sqrt{5(1+\tau^2)} \approx 1.231/a,$$

$$K_{D2} = \tau K_{D1} \approx 1.992/a. \tag{6}$$

The wave vectors of a QP lattice are shifted when the QP lattice is transformed into an approximant. The latter is obtained, in the present case, by substituting τ with F_{n+1}/F_n.[9] The approximant and the QP lattice wave vectors considered above are related to each other through the relations

$$\mathbf{K}_{D1}^n = \frac{\sqrt{5}F_n}{\tau^n}\mathbf{K}_{D1},$$

$$\mathbf{K}_{D2}^n = \frac{\sqrt{5}F_{n+1}}{\tau^{n+1}}\mathbf{K}_{D2}. \tag{7}$$

It is straightforward, taking into account Eq. (5), to check that $\mathbf{K}_{D1}^n$ and $\mathbf{K}_{D2}^n$ tend to $\mathbf{K}_{D1}$ and $\mathbf{K}_{D2}$ for n tending to infinity, i.e., F_{n+1}/F_n tending to τ. The vectors $\mathbf{K}_{D1}^n$ and $\mathbf{K}_{D2}^n$ of the approximants considered here are, thus, derived from the wave vectors $\mathbf{K}_{D1}$ and $\mathbf{K}_{D2}$ of the QP structures. The same argument holds for $-\mathbf{K}_{D1}^n$ and $-\mathbf{K}_{D2}^n$, which are derived from $-\mathbf{K}_{D1}$ and $-\mathbf{K}_{D2}$.

More notably, $\mathbf{K}_{D1}^n$ and $\mathbf{K}_{D2}^n$ are parallel to "ribbons" formed by oblate and prolate rhombi that lie parallel to the long diagonal of the rhombus unit cell. One of the ribbons is shadowed in Fig. 1(a). The relative occurrence frequencies for the oblate and prolate rhombi in such ribbons for an approximant of order (n',n) are $F_{n-1}:F_{n-2}$. The vector $\mathbf{K}_{D1}^n$ has its magnitude equal to the inverse of the average distance $\bar{d}^n$ between the line segments in the ribbons, $\bar{d}^n = 1/K_{D1}^n = H_n/2F_n$ [$\bar{d}^5 \approx 0.806a$ and $\bar{d}^6 \approx 0.815a$ for the (4,5) and (5,6) approximants]. In an infinite size QP lattice, the average distance between the line segments along a ribbon parallel to $\mathbf{K}_{D1}$ is, thus, exactly the inverse of K_{D1},

$$\bar{d} = \frac{1}{K_{D1}} \approx 0.812a. \qquad (8)$$

The wave vector $\mathbf{K}_{D2}$, from which $\mathbf{K}_{D2}^{n}$ is derived, corresponds to a higher order reflection along the same ribbons, its magnitude K_{D2} being exactly τ times greater than K_{D1}.

Indeed, the ten wave vectors on each of the two pseudodecagonal rings for the three approximants are derived from the ten wave vectors of each of the vector sets $\mathbf{K}_{\{0,1,1,\bar{1},\bar{1}\}}$ and $\mathbf{K}_{\{0,2,1,\bar{1},\bar{2}\}}$ of the QP structures, where these vectors correspond to strong-intensity Fourier components, and, as mentioned above, point to the vertices of two perfect decagons. In other words, for approximant structures of increasing order, the pseudodecagonal rings in the Fourier transforms will increasingly approach perfect decagonal ones. The wave vectors of the sets $\mathbf{K}_{\{0,1,1,\bar{1},\bar{1}\}}$ and $\mathbf{K}_{\{0,2,1,\bar{1},\bar{2}\}}$ are each parallel to a family of ribbons in the QP lattice, with their magnitudes inversely proportional to the average inter-line-segment distance along the ribbons (with respective coefficients 1 and τ for the two sets). However, unlike the two pairs of wave vectors $\pm\mathbf{K}_{D1}$ and $\pm\mathbf{K}_{D2}$ considered above, the shifts are not purely radial for the other eight vectors in each set when passing to the approximant structures. As a matter of fact, in the reciprocal space, the QP lattice is described by the D_{10} group, with ten twofold axes perpendicular to the principal C_{10} axis, while the rhombus approximants are described by the D_2 group (the maximum subgroup compatible with the periodicity). So only two of the ten twofold axes, which are parallel to the diagonals of the rhombus unit cell, are preserved in the approximant structures. The $\mathbf{K}_{\{0,1,1,\bar{1},\bar{1}\}}$ and $\mathbf{K}_{\{0,2,1,\bar{1},\bar{2}\}}$ vector sets lie parallel to five of the ten twofold axes of the QP structure, among which only the twofold axis parallel to the rhombus long diagonal is preserved, the four others are all broken. The vector shifts are, however, very weak. As shown in Table I, the shifts are less than 2% and 1% in magnitude for, respectively, the (4,5) and (5,6) approximants.

The above analysis shows that the Fourier components of the dielectric function, responsible for the main band gap opening in the approximant structures, are of the same origin in the QP structures. Consequently, pseudo-Brillouin zones can be defined for the QP structures upon these two wave-vector sets ($\mathbf{K}_{\{0,1,1,\bar{1},\bar{1}\}}$ and $\mathbf{K}_{\{0,2,1,\bar{1},\bar{2}\}}$) in the form of perfect decagons. The wave-vector shifts being weak in passing from QP to approximant structures, the parent QP structures will display similar photonic bands gaps as the approximant structures.

In a QP lattice, the average inter-line-segment distance in a ribbon is determined by the heights of the oblate and prolate tiles, and the spatial distribution of ribbons by the global average symmetry. Further, planes passing by infinite high scatterer axes and line segments in ribbons that are parallel to each other can be defined. The main band gap is, therefore, related to the average distance between these planes in the QP dielectric media, and determined by fundamental lattice parameters through global average structure orders. This point can also be compared to the case of the octagonal QP structure,[4] where the band structure is not significantly modi-
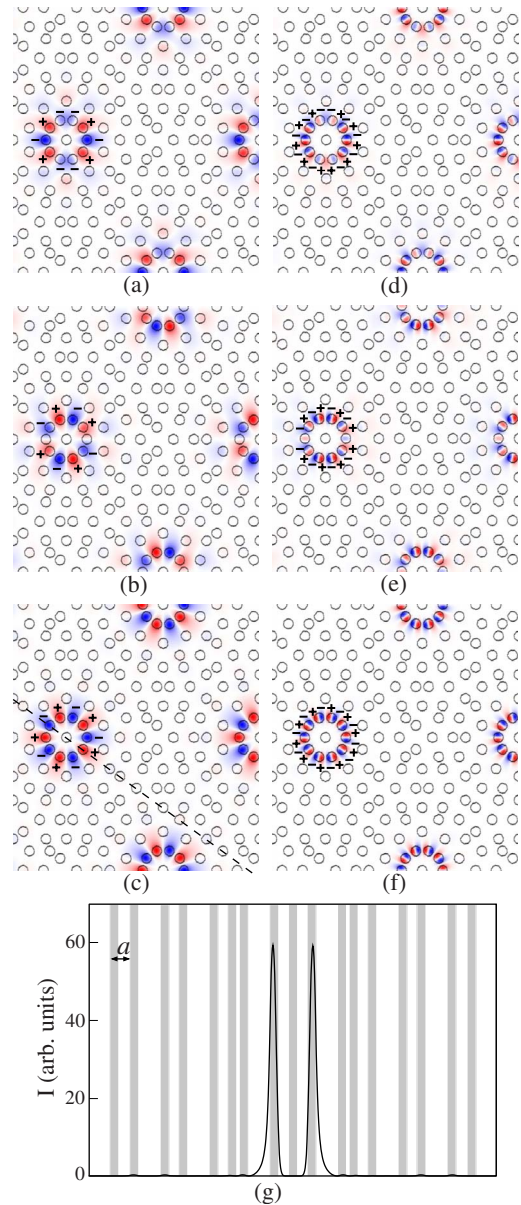
FIG. 4. (Color online) Electric-field patterns for the localized modes inside [(a)–(c)] the first and [(d)–(f)] second main photonic band gaps of the (5,6) decagonal approximant [see Fig. 2(c)]. The "+" and "−" signs indicate the field polarities. The field intensity of (c) along the dashed line is displayed in (g), where the shadowed zones represent the cross sections of the scatterers.

fied by the introduction of structure disorders since the structure randomization through tile flips does not modify the global average structure order.

B. Localization

Let us now consider the modes inside the main photonic band gaps for the decagonal approximant [Fig. 2(c)]. The corresponding electric-field patterns are displayed in Figs. 4(a)–4(f). It is obvious that for these modes, the field is localized on the decagonal ring, contrary to the work in Ref. 3 which concluded that localization effect is absent in the de-

TABLE II. The character table of D_{10} group. The characters of the Γ_S and Γ_T representations are also listed.

D_{10}	E	$2C_{10}$	$2C_5$	$2C_{10}^3$	$2C_5^2$	C_2	$5C_2'$	$5C_2''$
$\Gamma_1(A_1)$	1	1	1	1	1	1	1	1
$\Gamma_2(A_2)$	1	1	1	1	1	1	-1	-1
$\Gamma_3(B_1)$	1	-1	1	-1	1	-1	1	-1
$\Gamma_4(B_2)$	1	-1	1	-1	1	-1	-1	1
$\Gamma_5(E_1)$	2	τ	τ^{-1}	$-\tau^{-1}$	$-\tau$	-2	0	0
$\Gamma_6(E_2)$	2	τ^{-1}	$-\tau$	$-\tau$	τ^{-1}	2	0	0
$\Gamma_7(E_3)$	2	$-\tau^{-1}$	$-\tau$	τ	τ^{-1}	-2	0	0
$\Gamma_8(E_4)$	2	$-\tau$	τ^{-1}	τ^{-1}	$-\tau$	2	0	0
Γ_S	10	0	0	0	0	0	2	0
Γ_T	10	0	0	0	0	0	-2	0

cagonal structures. The electric field of the highest frequency mode in the first gap has a decapole distribution, while that in the second gap has an icosapole distribution. The other two modes in each gap have lower frequency levels which are close to each other and are characterized by electric-field distributions orthogonal to each other. The field intensity on the decapole, along a row of scatterers and normalized to unity on an area of a^2, is displayed in the same figure [Fig. 4(g)]. Obviously, the field intensity is confined in the ring and is characterized by a Gaussian-like distribution on the scatterers, with a peak width corresponding roughly to the cylinder diameter. Such localization effect is absent in the two regular Penrose-tiling approximants.

This localization effect in the decagonal approximant can be analyzed in the nearest-neighbor resonance framework, and these modes can be considered as various resonant states on the decagonal ring. Indeed, the decagonal ring is described by the D_{10} group, whose character table is given in Table II. Here, we are interested in the s and the tangential p (denoted as p_T) modes on the scatterers. The characters of their respective representations, namely, Γ_S and Γ_T, are given in the same table.

Under D_{10} group, the Γ_S and Γ_T representations can be decomposed in the following way:

$$\Gamma_S = \Gamma_1 + \Gamma_3 + \Gamma_5 + \Gamma_6 + \Gamma_7 + \Gamma_8, \tag{9}$$

$$\Gamma_T = \Gamma_2 + \Gamma_4 + \Gamma_5 + \Gamma_6 + \Gamma_7 + \Gamma_8, \tag{10}$$

where Γ_1 and Γ_3 describe, respectively, the bonding and antibonding states of the s wave; Γ_2 and Γ_4 those of the p_T wave. The other states are all doubly degenerate partially

bonding (Γ_5 and Γ_6) and partially antibonding (Γ_7 and Γ_8) states, and there are no nonbonding states under D_{10} group. For the three localized modes inside the first band gap, the field patterns in Figs. 4(a) and 4(b) are both described by the Γ_8 representation for the s wave, while that in Fig. 4(c) by the Γ_3 representation for the s wave. As far as the three modes inside the second gap are concerned, the field patterns in Figs. 4(d) and 4(e) are both described by the Γ_8 representation for the p_T wave, while that in Fig. 4(f) by the Γ_4 representation for the p_T wave. Their corresponding frequencies are given in Table III, where Γ_8' and Γ_8'' stand for the two doubly degenerate partially antibonding states described both by the Γ_8 representation.

In the nearest-neighbor approximation, the interscatterer interaction is described by a coupling parameter g that is proportional to $\langle \phi_n^* | H | \phi_{n+1} \rangle$, with $|\phi_n\rangle$ the wave function on the nth scatterer and H the Hamiltonian. The energy levels can be calculated using Hückel theory.[12] For weak g value, we obtain the frequency levels on a decagonal ring

$$\omega = \omega_0 + g, \quad \omega_0 + \frac{\tau}{2}g, \quad \omega_0 + \frac{\tau-1}{2}g, \quad \omega_0 - \frac{\tau-1}{2}g,$$

$$\omega_0 - \frac{\tau}{2}g, \quad \omega_0 - g, \tag{11}$$

where ω_0 stands for the mode frequency of an isolated individual scatterer. These frequency levels correspond, respectively, to those of Γ_1 (Γ_2), Γ_5, Γ_6, Γ_7, Γ_8, and Γ_3 (Γ_4) states for, respectively, the s and p_T waves.

TABLE III. The frequency levels of the s and p_T modes inside the two main photonic gaps. The first two Mie resonance frequencies are also listed.

	s and p_T mode frequencies		
	Γ_8'	Γ_8''	Γ_3	Γ_4	Mie frequencies
Γ_S	0.27	0.27	0.29		$\bar{\omega}_{Mie_1}$	0.19
Γ_T	0.52	0.52		0.54	$\bar{\omega}_{Mie_2}$	0.43

Equation (11) implies, for the Γ_3 (Γ_4) and Γ_8 modes of the s and p_T waves, the relation between the frequency levels

$$\left. \frac{\bar{\omega}_{\Gamma_3} - \bar{\omega}_0}{\omega_{\Gamma_8} - \bar{\omega}_0} \right|_s = \left. \frac{\bar{\omega}_{\Gamma_4} - \bar{\omega}_0}{\omega_{\Gamma_8} - \bar{\omega}_0} \right|_{p_T} = \frac{2}{\tau}. \qquad (12)$$

As mentioned above, nonbonding states are not compatible with the decagonal symmetry; there are, thus, no resonant states with frequency levels $\bar{\omega} = \bar{\omega}_0$ on the decagonal ring. Let us consider the case of an individual scatterer with the same dielectric constant. As a matter of fact, the first two Mie resonances[13] occur for an infinite cylinder of $\epsilon = 13$ for the size parameter $x = 2\pi r / \lambda = 0.29$ and 0.65, with λ the incident wavelength. This corresponds to the frequencies $\bar{\omega}_{Mie_1} = 0.19$ and $\bar{\omega}_{Mie_2} = 0.43(\omega a / 2\pi c)$. Taking these two frequencies for the s and p_T wave frequencies on an individual scatter, $\bar{\omega}_{Mie_1} = \bar{\omega}_0|_s$, $\bar{\omega}_{Mie_2} = \bar{\omega}_0|_{p_T}$, the values in Table III follow closely the relations given by Eq. (12). Therefore, the modes in the first gap can be considered as the antibonding (Γ_3) and partially antibonding (Γ_8) states between the ten scatters, each in the first Mie resonant state. Those in the second gap, the antibonding (Γ_4) and partially antibonding (Γ_8) states between the same scatters in the second Mie resonant state.

Now let us consider the group velocities of the localized modes inside the photonic gaps of the decagonal approximant. The group velocities of the Γ_8', Γ_8'', Γ_3, and Γ_4 states are displayed in Fig. 5. Strong velocity reductions can be observed for these modes. Indeed, for the three localized modes inside the first gap (the Γ_8', Γ_8'', and Γ_3 modes), the light group velocities are four magnitudes lower than that in vacuum. As a comparison, the group velocities of the low gap edge bands of all the three approximants are plotted in the same figure. It is clear that these velocities (the lowest among the bands below the first gap) are two magnitudes higher than those of the localized modes. Similar behaviors are obtained for the localized modes inside the second gap (the Γ_8', Γ_8'', and Γ_4 modes), where the Γ_4 mode corresponds to a still lower group velocity ($<10^{-6}c$), while those of the low gap edge bands for all the three approximants are at least 3 magnitudes higher.

Figure 5 shows clearly the role played by the local structures on the light wave propagation. Indeed, for the decagonal approximant, the strong group velocity reduction is obtained for the localized modes on the local tenfold symmetry patterns, while the group velocities of the low gap edge bands are not significantly affected by the local structure differences and remain comparable to those of the regular Penrose-tiling approximants. Moreover, we should be aware that, here, the group velocities are calculated on approximant structures. So they will be reduced as well following the diminution of the Brillouin zone size with increasing approximant order when approaching the QP structure. The comparison of these approximant structures of different orders and/or sizes allows to discern the group velocity reduction associated with local scale localization. Indeed, as exemplified by the low gap edge bands, the velocity difference due to the unit cell size increase in passing from the (4,5) to the
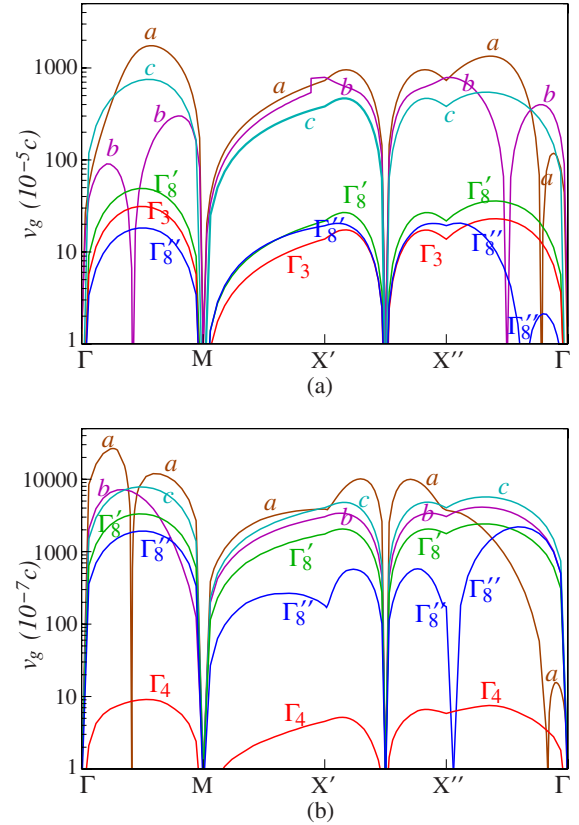
FIG. 5. (Color online) (a) Group velocities for the low-edge bands of (a and b) the (4,5) and (5,6) approximants of the regular Penrose tiling and (c) the (5,6) approximant of the decagonal tiling at the first main photonic gap edge, and those of the three modes (Γ_8', Γ_8'', and Γ_3) inside the same gap of the decagonal (5,6) approximant. (b) Group velocities for the low-edge bands of the same approximants (a–c) at the second main-gap edge and the three modes (Γ_8', Γ_8'', and Γ_4) inside the same gap of the decagonal (5,6) approximant.

(5,6) approximants is much weaker than the velocity reduction due to the localization on the tenfold patterns.

IV. DISCUSSION

The analysis on these dielectric systems show that the main photonic band-gap structures are determined by the global structure orders of the QP media. As a matter of fact, the gaps are related to the average distance between the planes passing by the dielectric scatterers as well as to the tenfold plane orientation symmetry (the decagonal bond-orientational symmetry), which are determined by fundamental lattice parameters of the QP lattices. The related wave vectors, corresponding to strong-intensity components in the Fourier spectra of the QP lattices, are only affected little when passing to the approximant structures, where similar photonic band gaps are obtained. This result can be compared to the case of the lowest photonic band gap in the octagonal dielectric structures studied previously.[2] Analogous effects are well known concerning the electronic pseudogaps in the quasiperiodic alloys.[14] Moreover, for the

regular and decagonal approximants of the same order, the photonic bands have similar structures as well outside the gaps. This can also be related to the global structure orders. Indeed, as indicated by Figs. 3(b) and 3(c), these structures display the same strong-intensity components. Light waves are only weakly scattered on the other components, and their propagation is not substantially affected by the local structure configuration differences.

As compared to previous works on Penrose-tiling-related dielectric structures,[3,5] we show that local structure configurations play an important role on the field distribution at certain frequencies. High degree of symmetry of local patterns implies short interscatterer distance and high neighbor scatterer number, favoring thus strong resonances between neighbor scatterers on such patterns. Indeed, Mie states decay asymptotically as $1/r$, the interaction between neighbor scatterers increases with decreasing interscatterer distance. In the decagonal structure, the ten scatterers on the decagonal ring are separated by an interscatterer distance of $(\tau-1)a \approx 0.618a$, which is much weaker than the other interscatterer distance a, as well as an average interplane distance $\bar{d} \approx 0.812a$. The interscatterer interaction is, thus, stronger on the decagonal rings as compared to the surrounding regions. As far as the regular Penrose tiling is concerned, there are five scatterers on the most symmetrical local patterns, i.e., the pentagonal rings; the interscatterer distance on the ring is $(\sqrt{3-\tau})a \approx 1.176a$, which is larger than a and $\bar{d}$. The interscatterer interaction on the pentagonal ring is, therefore, weaker as compared to the surrounding regions, disfavoring localization effect on the pentagonal rings.

High degree of local symmetry favors light localization on local structure patterns by leading to upshifts of frequency levels for the antibonding resonant states, among which those falling into the photonic band gaps correspond to the localized photonic modes. However, we should be aware that the localization effect depends, in turn, on the gap positions that are determined by the global structure order. As a matter of fact, a series of resonant modes are generated on the decagonal ring [Eq. (11)], among which well defined localized states are obtained only for those with high enough frequencies so that they can be shifted into the photonic band gaps. The lower frequency modes below the gap edges are susceptible to coupling with extended wave modes of close frequencies.

The relation between photonic band gaps and localized modes is further illustrated by the difference between the decagonal and octagonal structures. For the latter, only one localized mode (the highest frequency antibonding state) of each s and p waves is obtained, with the frequency level lying at the *low gap edges*.[4] For the decagonal structure, however, several localized resonant modes of both the s and p waves are shifted *inside* the gaps, allowing direct evaluation of the frequency level relations [Eq. (12)] for this structure. This is obviously related to the higher degree of symmetry of the decagonal structure, where the shorter interscatterer distance on the decagonal ring implies stronger interaction between neighbor scatterers and a stronger frequency increase for the antibonding states. Indeed, for the same tile edge length a, the interscatterer distance on the

decagonal ring $[(\tau-1)a \approx 0.618a]$ is about 20% weaker than that on the octagonal ring in the octagonal structure $[(\sqrt{2-\sqrt{2}})a \approx 0.765a]$. For a given average dielectric constant $\bar{\epsilon}$ value, the photonic gap midfrequency is inversely proportional to the average interplane distance $\bar{d}$. For the two structure families, $\bar{d}$ has comparable values $[\bar{d}=2a/(1+\sqrt{2}) \approx 0.824a$ for the octagonal QP lattice and $\bar{d} \approx 0.812a$ for the decagonal QP lattice]. Indeed, for an octagonal QP structure with tile edge length a and with the same average dielectric constant $\bar{\epsilon}$ as the decagonal structure, photonic band gaps of similar widths and midgap frequencies as compared to the decagonal structure are obtained. The interscatterer coupling is stronger on the local ring patterns in the decagonal structure, leading to higher resonance frequencies for the antibonding states on the rings and, thus, localized modes inside the gaps.

It is also worth noting that the midgap frequency scales inversely with $\sqrt{\epsilon}$, thus it is inversely correlated with the scatterer size in a 2D structure, while the Mie resonance frequency levels scale inversely with the scatterer size. The same localization effect should, therefore, last for weaker filling rate. To illustrate this, let us consider the three localized states Γ_8', Γ_8'', and Γ_3 inside the first photonic gap. Indeed, for the cylinder radius reduced to half of its initial value ($r=0.12a$), the corresponding filling rate is reduced to $f \approx 5.6\%$ for the (5,6) decagonal approximant, for which the first gap is shifted to a midfrequency of $\omega_{mid} \approx 0.46(\omega a/2\pi c)$. We can check that the three localized states are shifted to higher frequencies as well and remain inside the gap. As far as the scatterer dielectric constant ϵ value is concerned, as mentioned above, the gap midfrequency scales inversely with $\sqrt{\epsilon}$, and the Mie resonance frequency levels are inversely correlated with $\sqrt{\epsilon}$. Therefore, the presence of localized states inside the photonic gaps can persist as well down to rather weak ϵ values. Let us still consider the three localized states inside the first photonic gap. The first Mie resonance is described by a well defined peak in the scattering coefficient for dielectric constant down to about 5. For the same (5,6) decagonal approximant formed by dielectric cylinders of $\epsilon=5$, the first photonic gap is shifted to $\omega_{mid} \approx 0.45(\omega a/2\pi c)$. The three localized states are still obtained inside the gap.

V. CONCLUSION

In summary, light wave states in quasiperiodic Penrosey-tiling-related dielectric media that display similar long-range orders and different local configurations are comparatively studied through investigations on the respective approximant structures. Quasiperiodic structure effects on light wave behaviors at long- and short-range structure scales are analyzed, and relations between mechanisms underlying photonic gap opening and light wave localization are discussed. This study shows that local resonance induced light localization on maximum symmetry centers can, indeed, be a general phenomenon in quasiperiodic dielectric media, with the localized mode frequency levels relative to the photonic band gaps, depending on the system symmetry.

*wang@lps.u-psud.fr

[1] Y. S. Chan, C. T. Chan, and Z. Y. Liu, Phys. Rev. Lett. **80**, 956 (1998); S. David, A. Chelnokov, and J. Lourtioz, Opt. Lett. **25**, 1001 (2000).

[2] K. Wang, S. David, A. Chelnokov, and J. Lourtioz, J. Mod. Opt. **50**, 2095 (2003).

[3] Y. Wang, X. Hu, X. Xu, B. Cheng, and D. Zhang, Phys. Rev. B **68**, 165106 (2003).

[4] K. Wang, Phys. Rev. B **73**, 235122 (2006).

[5] C. Jin, B. Cheng, B. Man, Z. Li, and D. Zhang, Phys. Rev. B **61**, 10762 (2000); M. A. Kaliteevski, S. Brand, R. A. Abram, T. F. Krauss, P. Millar, and R. M. De La Rue, J. Phys.: Condens. Matter **13**, 10459 (2001).

[6] M. Notomi, H. Suzuki, T. Tamamura, and K. Edagawa, Phys. Rev. Lett. **92**, 123906 (2004).

[7] M. Bayindir, E. Cubukcu, I. Bulu, and E. Ozbay, Phys. Rev. B **63**, 161104(R) (2001).

[8] M. V. Jarić, Phys. Rev. B **34**, 4685 (1986).

[9] H. Zhang and K. H. Kuo, Phys. Rev. B **42**, 8907 (1990); see also K. Edagawa, K. Susuki, M. Ichihara, and S. Takeuchi, Philos. Mag. B **64**, 629 (1991).

[10] G. Entin-Wohlman, M. Kléman, and A. Pavlovitch, J. Phys. (Paris) **49**, 587 (1988).

[11] R. Ingalls, Acta Crystallogr., Sect. A: Found. Crystallogr. **A48**, 533 (1992).

[12] See R. G. Parr, *Quantum Theory of Molecular Electronic Structure* (Benjamin, New York, 1963), Chap. III.

[13] See C. F. Bohren and D. R. Huffman, *Absorption and Scattering of Light by Small Particles* (Wiley, New York, 1983), Chap. 4 and Appendix C.

[14] See, for example, K. Wang and P. Garoche, Phys. Rev. B **55**, 250 (1997).